



Research paper

Structure-based optimization of FDA-approved drug methylene blue as a *c-myc* G-quadruplex DNA stabilizer

Daniel Shiu-Hin Chan^{a,1}, Hui Yang^{a,1}, Maria Hiu-Tung Kwan^{a,1}, Zhen Cheng^a, Paul Lee^a, Li-Ping Bai^b, Zhi-Hong Jiang^b, Chun-Yuen Wong^c, Wang-Fun Fong^b, Chung-Hang Leung^{b,*}, Dik-Lung Ma^{a,*}

^a Department of Chemistry, Hong Kong Baptist University, Kowloon Tong, Hong Kong, China

^b Centre for Cancer and Inflammation Research, School of Chinese Medicine, Hong Kong Baptist University, Kowloon Tong, Hong Kong, China

^c Department of Biology and Chemistry, City University of Hong Kong, Tat Chee Avenue, Kowloon, Hong Kong, China

ARTICLE INFO

Article history:

Received 13 August 2010

Accepted 24 February 2011

Available online 4 March 2011

Keywords:

c-myc G-quadruplex

Methylene blue

FDA-approved drug

Repurposing

Structure-based optimization

ABSTRACT

G-quadruplexes are non-canonical DNA secondary structures putatively present in the promoter regions of oncogenes in the human genome. The targeting of promoter G-quadruplex structures to repress oncogene transcription represents a potential anticancer strategy. Here, we have used high-throughput virtual screening to identify FDA-approved drug methylene blue (MB) as a promising scaffold for binding the *c-myc* oncogene G-quadruplex DNA. Based on molecular docking analysis of MB to the *c-myc* G-quadruplex, we designed and screened 50 MB derivatives containing side chains that could interact with the G-quadruplex grooves. As a proof-of-concept, the highest-scoring compounds were synthesized and the interactions with the *c-myc* G-quadruplex were investigated using the FID assay. The results showed that the methylene blue derivatives **6a–c** were able to bind to the *c-myc* G-quadruplex with greater binding affinity compared to the known G-quadruplex binding ligand, crystal violet. The activity of the most potent compound identified from the FID assay, **6b**, as an inhibitor for polymerase-drive DNA extension was examined using a PCR-stop assay and compared against that of the parent compound methylene blue. The results of the PCR-stop assay showed that the addition of the side chain improved the activity of the derivatives as an inhibitor compared to the parent compound. The MB derivative **6b** was shown to be highly selective towards *c-myc* G-quadruplex over double-stranded DNA and other biologically relevant G-quadruplexes using UV–visible spectroscopy and mass spectrometry, respectively. The MB derivative **6b** could induce or stabilize *c-myc* G-quadruplex formation in both cell-free and cellular biological models, and displayed higher cytotoxicity against human hepatocarcinoma cells compared to the parent compound, MB.

© 2011 Elsevier Masson SAS. All rights reserved.

1. Introduction

G-quadruplexes are DNA secondary structures formed from planar arrangements of four guanines stabilized by Hoogsteen hydrogen bonding and monovalent cations [1]. G-quadruplexes have received much attention recently due to their putative existence in telomeres and in the promoter regions of oncogenes such as *c-myc* [2]. These non-canonical DNA secondary structures have emerged as a potentially new avenue for therapeutic intervention

of cancers [3]. Small molecules that can stabilize the G-quadruplex secondary structure could act as chemotherapeutic agents by inhibiting telomerase activity or by blocking oncogene transcription [3]. Quarfloxin (CX-3543), a first-in-class G-quadruplex-binding chemotherapeutic drug that has entered Phase II clinical trials for chronic lymphocytic leukaemia, is believed to exert its potent antitumour effects through disruption of the nucleolin/rDNA G-quadruplex complex in the nucleolus, arresting ribosomal RNA biogenesis [4].

The *c-myc* gene encodes a transcription factor that is understood to regulate 15% of all gene expression, including those involved in cell growth and apoptosis, and the overexpression of *c-myc* has been implicated in the tumorigenesis of malignant cancers [5]. The nuclease hypersensitivity element III₁ (NHE III₁) is a guanine-rich 27 base-pair sequence located upstream of the *c-myc* P1 promoter, and controls 80–90% of *c-myc* transcription [6]. Several

* Corresponding authors. Tel.: +852 3411 7075; fax: +852 3411 7348.

E-mail addresses: duncanl@hkbu.edu.hk (C.-H. Leung), edmondma@hkbu.edu.hk (D.-L. Ma).

¹ These authors contributed equally to the work.

² D.-L. Ma and C.-H. Leung contributed equally to this work.

small molecule ligands have been reported to stabilize the *c-myc* NHE III₁ G-quadruplex and inhibit *c-myc* oncogene transcription, including cationic porphyrins [7], quindoline derivatives [8] and platinum complexes [9]. We have recently identified a natural product-based *c-myc* G-quadruplex binder using high-throughput virtual screening [10a].

Pharmaceutical discovery and development is a highly difficult and expensive process. Repurposing is an attractive strategy whereby existing drugs are redeveloped for new uses [11]. With known pharmacokinetic and toxicological profiles, such drugs can enter Phase II clinical trials rapidly, allowing a 40% reduction in the overall cost due to the bypassing of preliminary assessments [12]. Furthermore, existing drugs tend to have more favourable absorption, delivery, metabolism and excretion (ADME) profiles. Consequently, marketed drugs can be considered to represent privileged scaffolds for the development of new therapeutics.

Structure-based design has emerged as a powerful tool in drug design and discovery, complementing existing combinatorial and high-throughput techniques [13]. By identifying potent small molecule binders *in silico*, the number of compounds to be tested *in vitro* can be vastly reduced. Abagyan and co-workers have identified nonsteroidal antiandrogens from a library of marketed oral drugs using high-throughput virtual screening [14]. Encouraged by these ideas, we set out to apply high-throughput virtual screening methods to identify interesting molecular scaffolds from existing drugs that could be developed as effective G-quadruplex binders. From the virtual screening results, we identified methylene blue (MB) as a promising candidate for further structure-based lead optimization (Fig. 1). MB contains a positively charged, aromatic scaffold suitable for G-quadruplex end-stacking. Functional groups can be attached to the parent MB scaffold to interact with the G-quadruplex grooves, increasing the binding affinity of the MB derivatives to the G-quadruplex. We report herein our structure-based lead optimization of FDA-approved drug MB as a *c-myc* G-quadruplex binding ligand. Using a unique *c-myc* NHE III₁ G-quadruplex model developed by our group, we designed and screened 50 MB derivatives containing various side chains for *c-myc* G-quadruplex binding ability. As a proof-of-concept of our approach, we synthesized the highest-scoring MB derivatives **6a–c** containing 4-bromophenyl moieties linked by short alkyl chains (Fig. 1). These analogues displayed improved *c-myc* G-quadruplex binding ability and selectivity profiles compared to the parent compound (MB), as demonstrated through spectroscopic experiments and *in vitro* biological assays.

2. Materials and methods

2.1. Materials

Calf thymus DNA (ct DNA) was purchased from Sigma Chemical Co. Ltd. and purified according to literature methodology [15a]. The

DNA per base-pair concentration was determined by UV–Vis absorption spectroscopy using the following molar extinction coefficient at the indicated wavelength: calf thymus DNA, $\epsilon_{260} = 13200 \text{ cm}^{-1} \text{ M}^{-1}$ (base-pair) [15b]. DNA oligomers were obtained from Tech Dragon Limited (Hong Kong). The sequence for oligomer Pu27 is [5'-TGGGGAGGGTGGGGAGGGTGGGGAAGG-3']. The intramolecular *c-myc* G-quadruplex structure was prepared by incubating Pu27 in Tris/KCl buffer, which was heated to 95 °C for 10 min and cooled to room temperature overnight. The expected G-quadruplex secondary DNA structure was confirmed by a positive CD peak at 262 nm and a negative CD peak at *ca.* 240 nm. Unless otherwise stated, spectroscopic titration experiments were performed in 10 mM Tris/HCl (pH 7.5) containing 10 mM KCl. Stock solutions of **6a–c** (10 mM) were made in dimethyl sulfoxide (DMSO). Further dilutions to working concentrations were prepared with double-distilled water. *Taq* DNA polymerase was purchased from QIAGEN (Valencia, CA, USA). Del 4 plasmid harbouring a 22-bp *c-myc* P1 promoter G-quadruplex forming sequence [5'-GGGGAGGGTGGGGAGGGTGGGG-3'] upstream of the luciferase reporter gene was obtained from Addgene (Cambridge, MA, USA). G4-mutant plasmid GM2 was kindly provided by Prof. Chowdhury (Proteomics and Structural Biology Unit, Institute of Genomics and Integrative Biology, CSIR, Delhi, India). Lipofectamine 2000 was obtained from Invitrogen. Passive Lysis Buffer and Luciferase Reporter Assay System were obtained from Promega (Madison, WI, USA). Methylene blue was obtained from Merck (Darmstadt, Germany). All other chemicals were obtained from Sigma–Aldrich (St. Louis, MO, USA).

2.2. Fluorescence intercalator displacement (FID) assay

The oligonucleotide Pu27 prior to use in the FID assay was annealed in a 10 mM TRIS buffer solution (pH 7.4, 100 mM KCl) by incubating at 95 °C for 10 min and cooled to room temperature gradually (0.1 °Cs⁻¹). To a solution of the annealed Pu27 (0.25 μM) and thiazole orange (0.5 μM, TO) in 20 mM TRIS buffer (pH 7.4, 100 mM KCl), an increasing amount of the appropriate methylene blue derivative was added and the emission spectrum was measured between 510 and 750 nm with an excitation wavelength of 501 nm using a PTI QM4 spectrometer. The area under the curve was determined using Graphpad Prism 5.0 which was then used to calculate the percentage of TO displacement using the following equation (1) [16]:

$$\% \text{TO displacement} = 100 - \left[\frac{\text{fluorescence area of sample}}{\text{fluorescence area of standard}} \times 100 \right] \quad (1)$$

where the fluorescence area of standard is defined as the area under the curve for an emission spectrum measured in the absence of methylene blue derivative. The DC₅₀ value was estimated by taking the first concentration after which the percentage displacement of TO is greater than or equal to 50%.

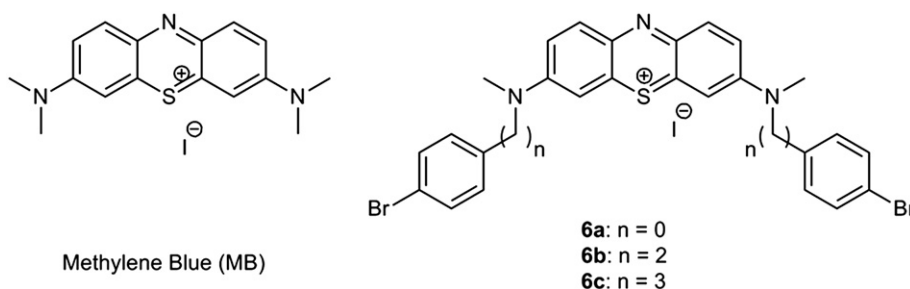


Fig. 1. The chemical structures of methylene blue (MB) and MB derivatives **6a–c**.

2.3. Absorption titration

Absorption spectra were recorded on a Perkin–Elmer Lambda 19 UV–Visible spectrophotometer. A solution of **6b** or MB (10 μ M) was prepared in Tris/HCl buffer (10 mM, pH 7.4) containing 10 mM KCl, and aliquots of a millimolar stock solution of Pu27 in Tris/KCl buffer were added. Absorption spectra were recorded in the spectral range $\lambda = 200$ –600 nm after equilibration at 20.0 °C for 10 min. The intrinsic binding constant, K , was determined from a plot of $D/\Delta\epsilon_{ap}$ vs D according to equation (2) [17]:

$$D/\Delta\epsilon_{ap} = D/\Delta\epsilon + 1/(\Delta\epsilon \times K) \quad (2)$$

where D is the concentration of DNA, $\Delta\epsilon_{ap} = |\epsilon_A - \epsilon_F|$, $\epsilon_A = A_{obs}[\text{ligand}]$, and $\Delta\epsilon = |\epsilon_B - \epsilon_F|$; ϵ_B and ϵ_F correspond to the extinction coefficients of DNA–ligand adduct and unbound ligand, respectively. Similar absorption titration experiments were performed using ct DNA.

2.4. PCR-stop assay

The PCR-stop assay was performed by using a modified protocol of the previously reported method [8]. The reactions (40 μ L) were performed in 1 \times PCR buffer, containing each pair of oligomers (10 mM), deoxynucleotide triphosphate (0.16 mM), *Taq* polymerase (2.5 U), and increasing concentrations of the compound (0–250 μ M). The reaction mixtures were incubated in a thermocycler under the following cycling conditions: 94 °C for 3 min followed by 30 cycles at 94 °C for 30 s, 58 °C for 30 s, and 72 °C for 30 s. The amplified products were resolved on 1.3% agarose gel and visualized by ethidium bromide staining.

2.5. Selectivity experiments using mass spectrometry

Stock solutions of all oligonucleotides (500 μ M) were prepared in ammonium acetate buffer (pH 7.6, 500 mM), stock solution of **6b** (400 μ M) was prepared in methanol. A solution (100 μ L) of the appropriate oligonucleotide (100 μ M, final concentration) and **6b** (200 μ M, final concentration) was prepared in 100 mM ammonium acetate buffer containing 50% methanol and left to stand at room temperature for 1 h and injected directly into the ESI–TOF–MS. The injection rate was 3 μ L min^{−1}. Each sample of DNA–**6b** complex solution was made in duplicate. ESI–TOF–MS experiments were conducted in the negative-ion mode with a Bruker micrOTOFQ mass spectrometer. All oligonucleotides were purchased from Invitrogen. The capillary voltage was set at +3500 V, and the dry N₂ gas flow was 4.0 L min^{−1} at 100 °C. Data were analyzed by the software Bruker Daltonics Data Analysis.

The oligonucleotide sequences used in the mass spectrometry experiments are shown below:

- (i) *c-myc*: 5'-TGGGGAGGGTGGGGAGGGTGGGGAAGG-3'
- (ii) *c-kit* 1: 5'-AGAGGGAGGGCGCTGGGAGGAGGGGCT-3'
- (iii) *c-kit* 2: 5'-CCCGGGCGGGCGGAGGAGGGGAGGT-3'
- (iv) truncated *bcl-2*: 5'-CGGGCGGGAGGAAGGGGGCGGGAGC-3'

2.6. Transfection and luciferase assay

Exponentially growing HepG2 cells cultured in DMEM media supplemented with 10% FBS were seeded in a 24-well plate on Day 1. Del 4 or G4-mutant plasmid GM2 (1 μ g) was transfected into the HepG2 cells growing at 75% confluency using Lipofectamine 2000 as per manufacturer's protocol. After 5 h of transfection, the cells were washed 1 \times with PBS and fresh media was added into each well. The cells were incubated with **6b** or MB (0–12.5 μ M) for 24 h.

The cells were lysed with 1 \times Passive Lysis Reagent buffer with continuous pipetting at room temperature for 30 min. The homogenate was centrifuged for 2 min at 10,000 g. The supernatant was used for protein estimation by Bicinchoninic Acid (BCA) method. Luciferase assay was performed for three biological replicates and luciferase activity was normalized by total protein concentration.

2.7. Cytotoxicity test (MTT assay)

HeLa cells were seeded in a 96-well flat-bottomed microplate at 8000 cells/well in growth medium solution (100 μ L; FBS (10%), L-glutamine (1%), and Penicillin streptomycin (1%) in MEM). Serial dilutions of compounds **6a** or MB were added to each well. The microplate was incubated at 37 °C in CO₂/air (95:5) in a humidified incubator for 24 h. After incubation, 3-(4,5-dimethylthiazol-2-yl)-2,5-diphenyl tetrasodium bromide (MTT) (10 μ L, 5 mg mL^{−1}) was added to each well. The microplate was reincubated at 37 °C in 5% CO₂ for 4 h. Solubilization solution (100 μ L; sodium dodecyl sulphate (10%), 10 mM HCl) was added to each well. The microplate was left in an incubator for 24 h. The absorbance at $\lambda = 570$ nm was measured by a microplate reader. The IC₅₀ values of the compounds were determined by the dose dependence of the surviving cells after exposure to the compounds for 24 h.

2.8. Synthesis

Compounds **2** [18] and **4b–c** [19] were synthesized according to literature procedures and the purity was confirmed by comparison with literature spectroscopic data. The amines **5b–c** were synthesized according to a general procedure and the purity of **5b** confirmed by comparison with literature spectroscopic data [20]. Compounds **1**, **3b–c** and **5a** were purchased from Sigma–Aldrich and used as received.

2.8.1. General procedure for **5b–c**

The appropriate iodide **5** (5 mmol) and aq. methylamine (40%, 60 mL) were stirred in THF at room temperature for 3 h. The volatiles were removed under reduced pressure. Then water (100 mL) was added, and the solution was acidified to pH 2 using 5 M HCl. The solution was washed with ether (2 \times 100 mL) and the aqueous layer was basified to pH 12 using 10 M NaOH. The solution was extracted with ether (2 \times 100 mL), and the organic layers were combined, dried (MgSO₄) and evaporated to give **6a** as a pale yellow oil (1.03 g, 4.8 mmol, 90%).

2.8.2. *N*-Methyl-2-(4-Bromophenyl)ethylamine (**5b**)

Yellow oil (1.03 g, 90%). ¹H NMR (300 MHz, CDCl₃): δ 7.42 (d, $J = 8.3$ Hz, 2H), 7.08 (d, $J = 8.3$ Hz, 2H), 2.85–2.72 (m, 4H), 2.43 (s, 3H), 1.25 (bs, 1H).

2.8.3. *N*-Methyl-2-(4-Bromophenyl)propylamine (**5c**)

Yellow oil (0.83 g, 89%). ¹H NMR (300 MHz, CDCl₃): δ 7.39 (d, $J = 8.3$ Hz, 2H), 7.06 (d, $J = 8.3$ Hz, 2H), 2.64–2.56 (m, 4H), 2.42 (s, 3H), 1.83–1.73 (m, 2H), 1.30 (bs, 1H). ¹³C NMR (100 MHz, CDCl₃): δ 140.9, 131.4, 130.1, 119.5, 51.1, 36.1, 32.9, 30.7. HR-MS (ESI–TOF) calcd. for C₁₀H₁₄BrN [M + H]⁺: 228.0387. Found: 228.0385.

2.8.4. General procedure for **6a–c** [21]

The appropriate amine (1.5 mmol) was added to a solution of phenothiazinium salt **2** (181 mg, 0.25 mmol) in MeOH (50 mL), and the reaction was stirred at room temperature for 40 min or until **3** was consumed as monitored by TLC (3% MeOH/CHCl₃). The solvent was removed under reduced pressure and the residue was redissolved in CH₂Cl₂. The solution was washed with 1% HCl (4 \times 50 mL)

and water (2 × 20 mL), and the organic layer was dried (MgSO₄) and concentrated *in vacuo*. The product was precipitated by the addition of ether and collected by filtration. Further purification if necessary could be carried out by flash column chromatography on silica gel (CHCl₃–3% MeOH/CHCl₃).

2.8.5. 3,7-Bis(4-bromophenylamino)phenothiazin-5-ium iodide (**6a**)

Purple powder (44 mg, 25%). ¹H NMR (500 MHz, CDCl₃): δ 8.08 (d, *J* = 2.4 Hz, 2H), 7.87 (d, *J* = 9.4 Hz, 4H), 7.70 (d, *J* = 8.6 Hz, 4H), 7.21 (d, *J* = 8.6 Hz, 4H), 7.09 (dd, *J* = 9.4, 2.4 Hz), 3.78 (s, 6H). ¹³C NMR (125 MHz, CDCl₃): δ 154.0, 143.1, 138.5, 137.6, 136.5, 134.3, 128.5, 123.0, 121.1, 108.0, 43.0. HR-MS (MALDI-TOF) calcd. for C₂₆H₂₀Br₂N₃SI [M⁺]: 565.9720. Found: 565.9733.

2.8.6. 3,7-Bis((4-bromophenylethyl)(methyl)amino)phenothiazin-5-ium iodide (**6b**)

Purple powder (30 mg, 16%). ¹H NMR (400 MHz, CDCl₃): δ 7.88 (d, *J* = 9.5 Hz, 2H), 7.70 (s, 2H), 7.43 (d, *J* = 8.3 Hz, 4H), 7.17–7.12 (m, 6H), 4.00 (t, *J* = 4.9 Hz, 4H), 3.25 (s, 6H), 3.04 (t, *J* = 4.9 Hz, 4H). ¹³C NMR (100 MHz, CDCl₃): δ 153.3, 138.5, 136.5, 136.1, 135.5, 132.0, 130.7, 128.1, 121.1, 107.1, 55.4, 41.1, 33.5. HR-MS (MALDI-TOF) calcd. for C₃₀H₂₈Br₂N₃SI [M⁺]: 622.0365. Found: 622.0356.

2.8.7. 3,7-Bis((3-(4-bromophenyl)propyl)(methyl)amino)phenothiazin-5-ium iodide (**6c**)

Purple powder (37 mg, 19%). ¹H NMR (400 MHz, CDCl₃): δ 7.90 (d, *J* = 9.6 Hz, 2H), 7.57 (s, 2H), 7.44 (d, *J* = 8.1 Hz, 4H), 7.15–7.12 (m, 6H), 3.73 (t, *J* = 6.7 Hz, 4H), 3.36 (s, 6H), 2.77 (t, *J* = 7.4 Hz, 4H), 2.10–2.05 (m, 4H). ¹³C NMR (100 MHz, CDCl₃): δ 153.5, 139.7, 138.8, 136.1, 135.4, 131.9, 130.5, 128.4, 120.3, 107.0, 53.4, 46.5, 32.4, 29.0. HR-MS (MALDI-TOF) calcd. for C₃₂H₃₂Br₂N₃SI [M⁺]: 650.0678. Found: 650.0682.

2.9. Molecular modelling

Molecular docking was performed by using the ICM-Pro 3.6-1d program (Molsoft) [22]. According to the ICM method, the molecular system was described by using internal coordinates as variables. Energy calculations were based on the ECEPP/3 force field with a distance-dependent dielectric constant. The biased probability Monte Carlo (BPMC) minimization procedure was used for global-energy optimization. The BPMC global-energy optimization method consists of: 1) a random conformational change of the free variables according to a predefined continuous probability distribution; 2) local-energy minimization of analytical differentiable terms; 3) calculation of the complete energy including non-differentiable terms such as entropy and solvation energy; 4) acceptance or rejection of the total energy based on the Metropolis criterion and return to step (1). The binding between the compounds and DNA was evaluated by binding energy, including grid energy, continuum electrostatic, and entropy terms. The initial model of loop isomer was built from X-ray crystal structures of human intramolecular telomeric G-quadruplex (PDB code: 1KF1) [23], according to a previously reported procedure [8,9]. Briefly, the structure of human intramolecular telomeric G-quadruplex was imported into Insight II package (Accelrys Inc., San Diego, CA), and necessary modifications were carried out including replacements and deletions of bases. Missing loop nucleotides were added using single-strand B-DNA geometry using the Biopolymer module. Potassium ions were placed between the G-tetrad planes to stabilize the tetrad structure. The initial models were then immersed in a box of TIP3P water molecules, and an appropriate number of sodium ions was added to neutralize the negative charge of the phosphate backbone. The molecular dynamics simulations were

carried out in NAMD with VMD monitoring the process. The CHARMM force field parameter was assigned to every atom, and the Particle Mesh Ewald electrostatics was used to compute long-range electrostatic interactions. Hydrogen atoms were added and minimized by 3000 steps of conjugate gradient minimization. After 4000 steps of conjugate gradient minimization, two stages of molecular dynamics simulations were carried out at 300 K. In the first stage, only the loop area atoms were allowed to move, and this process involved a 20 ps equilibration and 100 ps simulations. The second stage involved unrestrained molecular dynamics simulations with 20 ps equilibration and 100 ps simulations at 300 K. Trajectories were recorded every 0.1 ps, and the most stable structure was extracted and further refined by 2500 steps of conjugate gradient minimization. In the docking analysis, the binding site was assigned across the entire structure of the DNA molecule. The ICM docking was performed to find the most favourable orientation. The resulting trajectories of the complex between the compounds and G-quadruplex DNA were energy minimized, and the interaction energies were computed.

3. Results and discussion

3.1. Virtual screening of FDA-approved drug database

Despite the publication of a solution-based structure of *myc22* by Ambrus et al. [24], we have chosen to construct a model of the *c-myc* NHE III₁ G-quadruplex loop isomer using the X-ray crystal structure of the intramolecular human telomeric G-quadruplex DNA (PDB code: 1KF1) [15]. NMR structures of biomolecules are typically solved as a series of energy minimized conformations [24], and as a result, for a given NMR structure there are multiple conformations which needs to be considered during the virtual ligand screening process. This does not only decrease the accuracy of the virtual ligand screening, but also increases the computing resources required to undertake such a study. This NHE III₁ G-quadruplex loop isomer model has been previously employed to study the interaction between quindoline compounds [8] and the *c-myc* G-quadruplex. We have also used this model for the structure-based optimization of platinum(II) Schiff base complexes that has shown improved *c-myc* G-quadruplex binding activities compared to the parent hit compound [9]. In the present study, over 3000 compounds in a database of FDA-approved drugs were screened *in silico*. To our knowledge, this is the first large-scale application of high-throughput virtual screening of an approved drug database for *c-myc* G-quadruplex stabilizing ligands. The continuously flexible ligands were docked to a grid representation of the receptor and assigned a score reflecting the quality of the complex according to the ICM method [ICM-Pro 3.6-1d molecular docking software (Molsoft)] [22]. Based on the database of FDA-approved drugs, the phenothiazinium salt methylene blue (MB) emerged as an attractive candidate for further structural modification.

MB is a well-known DNA-intercalating chromophore that was originally developed as a dyestuff during the late nineteenth century. It possesses a broad range of biological activities, and has been used for the treatment of malaria, nitrate poisoning, methemoglobinemia, dementia and cancers through photodynamic therapy [25]. The interaction between MB and the tetramolecular human telomeric (5'-TTAGGG-3')₄ G-quadruplex has been studied by spectroscopic techniques, and a binding constant of approximately 1 × 10⁶ dm³ mol⁻¹ has been reported [26]. MB has also been reported to display binding to a few G-quadruplex forms, including the human telomeric sequence, as determined by competitive dialysis [27]. However, to our knowledge, MB has not yet been reported to be a *c-myc* G-quadruplex ligand, nor has the G-quadruplex-binding efficacy

of MB been evaluated in a biological system. Inspired by the phenothiazinium template, we endeavoured to synthesize a series of MB analogues as a proof-of-concept for our structure-guided lead optimization approach. As MB is an FDA-approved drug, we reasoned that it would be advantageous from a pharmacological point of view to develop analogues of the phenothiazinium template rather than of a heretofore unknown aromatic scaffold. Based on the phenothiazinium template, a total of 50 compounds were designed and screened *in silico* (Table S1). Of the 50 compounds screened the phenothiazinium-based compounds bearing the bromophenyl pendant linked by an aliphatic side chain showed the highest binding affinity as indicated by the negative binding energies. Based on the predicted binding energies from the *in silico* screening, we decided to synthesize the compounds **6a–c** and examine their interaction with the *c-myc* G-quadruplex.

3.2. Chemical synthesis

To synthesize methylene blue derivatives **6a–c**, a modification of Streckowski's procedure was used [21]. 10*H*-Phenothiazine **1** was first oxidised to phenothiazin-5-ium tetraiodide hydrate **2** using excess iodine in chloroform at 0 °C (Scheme 1). The periodide **2** was then reacted with amines **5a–c** in methanol to yield the MB derivatives **6a–c**, which could be isolated by aqueous workup followed by precipitation from a concentrated dichloromethane solution using diethyl ether. Further purification if necessary could be carried out by column chromatography on silica gel. The MB derivatives **6a–c** were obtained as dark purple solids that gave intense blue solutions upon dissolution. *N*-methylamines **5b–c** were synthesized *via* conversion of the commercially available alcohols **3b–c** to the corresponding iodides **4b–c** using the iodine/triphenylphosphine/imidazole system, followed by nucleophilic substitution with excess methylamine to afford the desired *N*-methylamines **5b–c** (Scheme 1).

We found that MB derivatives **6a–c** were prone to light-induced degradation. Therefore, these compounds were stored in the dark at –20 °C and stock solutions of compounds were freshly prepared before use in spectroscopic or biological experiments. As expected, MB derivatives **6a–c** exhibited reduced water solubility compared to the parent compound (MB) due to the presence of additional aliphatic and aromatic functional groups, but they could be dissolved at millimolar concentrations in aqueous solution containing 10% organic solvent. Stock solutions of **6a–c** were thus prepared at 10 mM concentration in DMSO and these could be diluted with aqueous buffer without any observable precipitation.

3.3. Fluorescence intercalator displacement (FID) assay

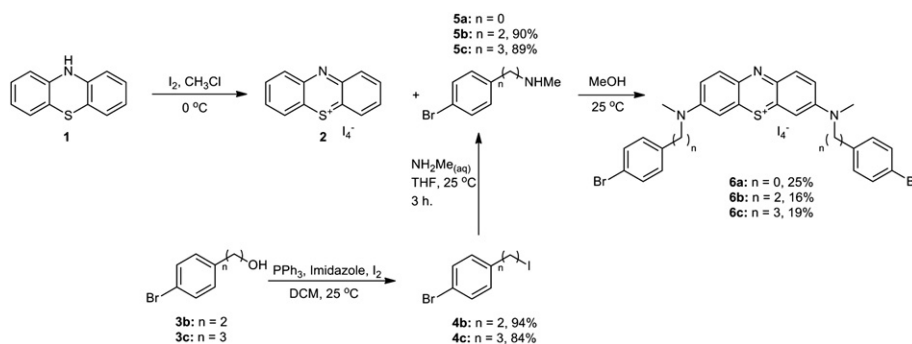
To determine the ability of the synthesized methylene blue derivatives **6a–c** to interact with the *c-myc* G-quadruplex,

a fluorescence intercalator displacement (FID) assay was performed using thiazole orange (TO) as the fluorophore (Fig. 2). Based on the concentrations of the MB derivatives **6a–c** that were required to reduce the TO fluorescence intensity by 50%, an indication of the binding affinity of the different MB derivatives **6a–c** towards the *c-myc* G-quadruplex could be determined. The concentrations at which the fluorescence of TO was reduced by 50% (DC₅₀) were estimated for the MB derivatives **6a–c** and the reported G-quadruplex binding ligand crystal violet (CV) (Fig. 2). The fluorescence spectrum and %TO displacement plots are shown in Figs. S1–S4.

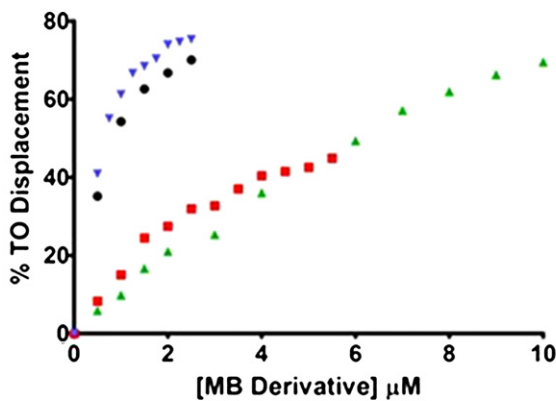
The DC₅₀ results shown in Fig. 2 show a trend that is consistent with the binding scores predicted by molecular modeling (Table S1). The methylene blue derivative **6a** was predicted to be the weakest *c-myc* G-quadruplex binder of the series, and this was reflected by a DC₅₀ value of >6 μM which is highest of the DC₅₀ values estimated from the FID assay. The most active compound predicted by molecular modeling, **6b**, showed a DC₅₀ of 0.75 μM suggesting that it has a higher binding affinity relative to CV based on a comparison of the DC₅₀ value estimated for CV under comparable conditions. It is worth noting that the trends in the binding energies were correlated with the binding affinity indicated by the DC₅₀ values of the MB derivatives **6a–c** estimated using the FID assay. This result validates the use of molecular modeling as a tool for the structure-based lead optimization of hit compounds.

3.4. PCR-stop assay

To provide additional validation of our molecular modelling results, a dose response experiment with **6b** was performed using the PCR-stop assay. In this cell-free assay, the compound was incubated with oligomer Pu27 and the complementary reverse primer in the presence of *Taq* polymerase. Stabilization of the intramolecular *c-myc* G-quadruplex structure by **6b** prevents hybridization of the complementary sequence. *Taq* polymerase is unable to recognize the G-quadruplex structure and DNA amplification is inhibited, which is manifested as a reduction in the 43 bp PCR product observed after agarose gel electrophoresis (Fig. 3). The results show that the addition of **6b** led to a dose-dependent decrease in the 43 bp PCR amplification product. Partial inhibition of *Taq* polymerase-mediated DNA amplification through stabilization of the *c-myc* G-quadruplex structure was observed at 100 μM of **6b** and complete inhibition at 250 μM. By comparison, MB was only slightly active at 250 μM (Fig. S5). This indicates that **6b** is able to induce or stabilize G-quadruplex formation in biological systems. Furthermore, this result confirms that the MB derivative **6b** binds more strongly to the *c-myc* G-quadruplex compared to the parent compound MB, which is in agreement with our molecular modeling calculations.



Scheme 1. Synthesis of methylene blue derivatives **6a–c**.



Compound	Average DC ₅₀ /μM ± SD ^a	Binding Score
6a	5.33 ± 0.76	-31.67
6b	0.75 ± 0.00	-49.87
6c	2.00 ± 0.86	-45.99
CV	4.00	

[a] the DC₅₀ values are estimated by taking the first concentration value where the displacement of TO is greater than 50%. The values for 6a, 6b and 6c are averaged over three trials and are expressed with standard deviations (SD)

Fig. 2. Plot of the percentage displacement of thiazole orange (TO) as a function of the concentration of: (a) 6a (●); (b) 6b (▼); 6c (■); and crystal violet (▲). Insert: Table showing the DC₅₀ values for the compounds 6a–c and crystal violet estimated from the fluorescence intercalator displacement assay. (For interpretation of the references to colour in this figure legend, the reader is referred to the web version of this article.)

3.5. Molecular modeling and lead optimization

We performed molecular modeling of MB with the NHE III₁ intramolecular G-quadruplex loop isomer model in order to investigate the mode of binding. The 1:2:1 loop isomer is the predominant isomer in the *c-myc* parallel G-quadruplex structure [28]. Since neither NMR nor X-ray crystallographic information for the NHE III₁ 1:2:1 loop isomer is available, a model was built from the known, closely related X-ray crystal structure of the human intramolecular telomeric G-quadruplex DNA. A truncated 18 base-pair sequence [5'-AGGGTGGGGAGGGTGGGG-3'] was used for this work since nucleotides G2–G5 in the *c-myc* sequence [5'-TGGGGAGGGTGGGGAGGGTGGGGAAGG-3'] are not involved in the G-quartet structure. The molecular docking results showed that the positively charged aromatic scaffold of MB is end-stacked at the 3'-terminus of the *c-myc* G-quadruplex, with a binding

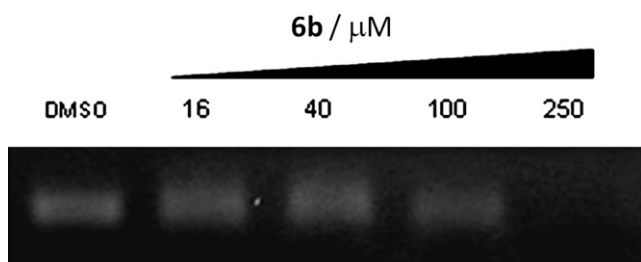


Fig. 3. Incubation of *c-myc* G-quadruplex oligomer: Pu27 with 6b (0–250 μM) caused a dose-dependent decrease of the PCR amplification product at 43 bp. Representative gel photograph image of replicate independent experiments shown.

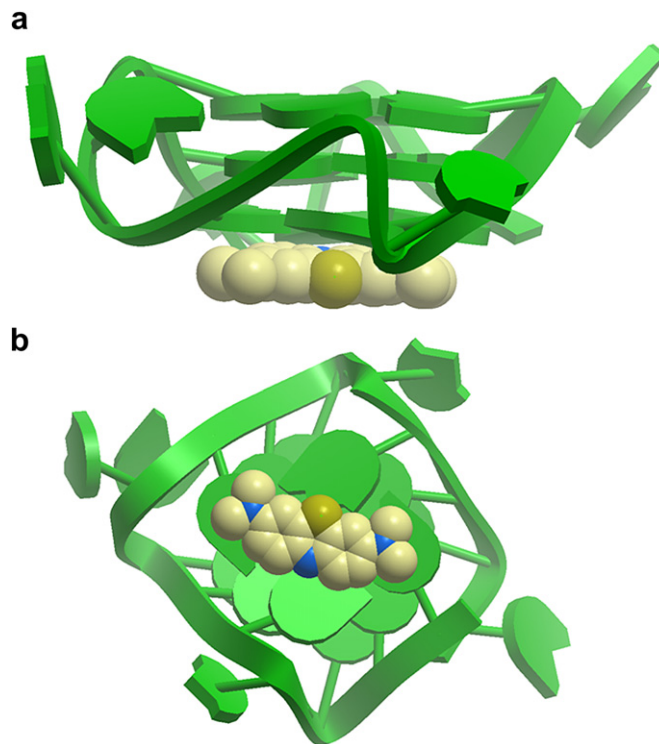


Fig. 4. Hypothetical molecular models showing the a) Side view; b) Top view of the interactions of MB with the *c-myc* G-quadruplex structure. The G-quadruplex is displayed as a ribbon representation (green), while MB is depicted as a space-filling representation showing carbon (beige), nitrogen (blue), sulphur (green-yellow) and bromine (purple) atoms. (For interpretation of the references to colour in this figure legend, the reader is referred to the web version of this article.)

energy of $-32.64 \text{ kcal mol}^{-1}$ (Fig. 4). We envisaged that the introduction of longer side chains at the amine position could increase the binding affinity and selectivity of the ligands for the *c-myc* G-quadruplex by increasing interactions with the grooves and loops of the G-quadruplex, which is a common strategy in the design of quadruplex-binding ligands [3].

We reasoned that longer side chains could interact with the grooves of the *c-myc* G-quadruplex, which could improve the binding potency and selectivity of the quadruplex ligands. We therefore designed over 50 MB derivatives containing side chains of various lengths and screened these compounds *in silico*. The 3,7-bis(dialkylamino)phenothiazin-5-ium derivatives 6a–c containing 4-bromophenyl substituents linked by short alkyl chains emerged as a promising series for *in vitro* testing. The bromide group serves as a useful functional handle for future structural modifications. Both derivatives showed higher molecular docking energies compared to MB, with 6b exhibiting the highest binding energy of $-49.87 \text{ kcal mol}^{-1}$, suggesting that a two-carbon unit is the optimum length for the linker. Compared to MB (Fig. 4), 6b is predicted to form more extensive π -stacking interactions with the G-quartet through its additional aromatic substituent (Fig. 5). Furthermore, the other aromatic ring of the phenothiazinium scaffold appears to contact the side loops of the G-quadruplex, potentially contributing favourable interactions to the binding energy. Notably, the binding energy for an intercalative binding mode is vastly higher for 6b ($+32.79 \text{ kcal mol}^{-1}$) compared to MB ($-13.66 \text{ kcal mol}^{-1}$), suggesting that the bulky side chains of 6b prevent intercalation into the G-quadruplex presumably due to steric effects (Fig. 6). Taken together, our molecular docking results suggest that the presence of the additional side chains on the phenothiazinium scaffold favour G-quadruplex end-stacking at

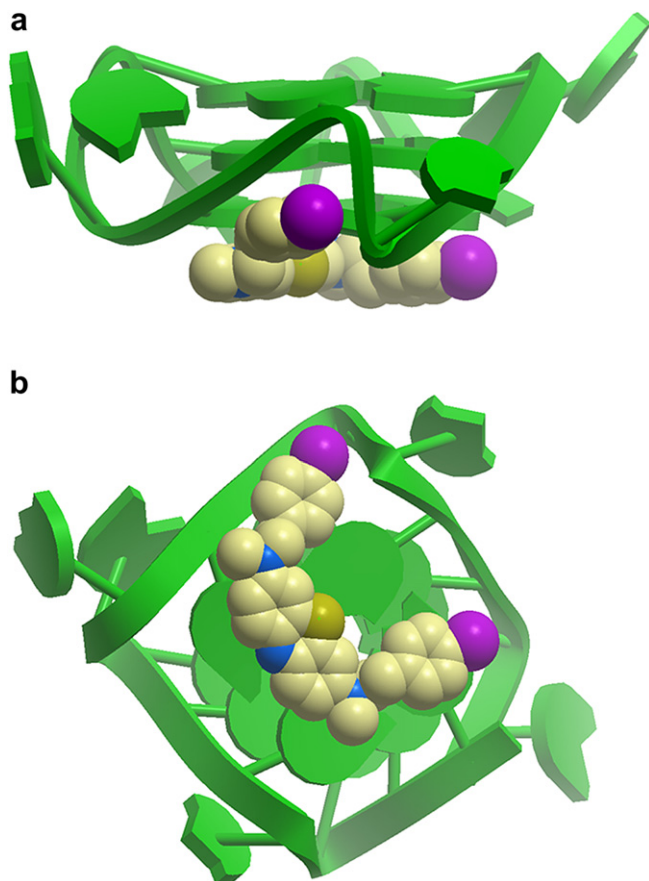


Fig. 5. Hypothetical molecular models showing the a) Side view; b) Top view of the interactions of **6b** with the *c-myc* G-quadruplex structure. The G-quadruplex is displayed as a ribbon representation (green), while **6b** is depicted as a space-filling representation showing carbon (beige), nitrogen (blue), sulphur (green-yellow) and bromine (purple) atoms. (For interpretation of the references to colour in this figure legend, the reader is referred to the web version of this article.)

the expense of intercalation. The molecular modeling calculations also predict that end-stacking of **6b** at the 5'-terminus ($-34.11 \text{ kcal mol}^{-1}$) is disfavoured relative to 3'-end stacking ($-49.87 \text{ kcal mol}^{-1}$).

3.6. Absorption titration

The abilities of methylene blue derivatives **6b** to bind *c-myc* G-quadruplex DNA were first studied by an absorption titration experiment. UV-visible spectrum of the MB derivative **6b** with increasing concentrations of the oligonucleotide Pu27 [5'-TG₄AG₃TG₄AG₃TG₄A₂G₂-3'] is shown in Fig. 7.

Hypochromic effects were observed in the UV-visible spectrum of **6b** with oligonucleotide Pu27, which is attributed to the strong

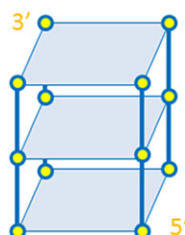


Fig. 6. Calculated binding energies (in kcal mol^{-1}) for **6b** bound to different sites of the intramolecular *c-myc* G-quadruplex.

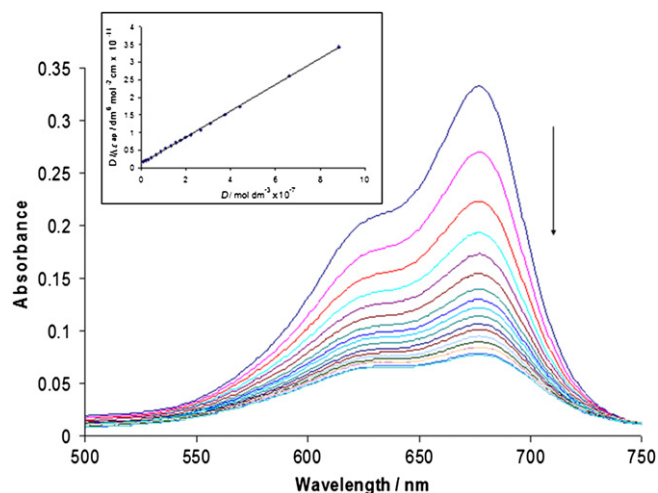


Fig. 7. UV-Vis absorption titration of **6b** ($1 \times 10^{-5} \text{ M}$) in Tris/KCl buffer (10 mM KCl, 10 mM Tris-HCl, pH 7.5) with increasing amounts of *c-myc* oligomer Pu27 ($0-8.8 \times 10^{-7} \text{ M}$). Inset: plot of $D/\Delta\epsilon_{ap}$ versus D . Absorbance was monitored at 678 nm.

interaction between **6b** and the G-quadruplex (Fig. 7). The absorbance of **6b** increased again upon addition of excess DNA (not shown), a phenomenon previously observed with MB and calf thymus (ct) DNA, suggesting the presence of more than one binding mode [24]. Nevertheless, a relative value for the binding constant could still be estimated from the initial decrease in absorbance [29] using the Scatchard equation [16]. We thus determined the binding constant K of **6b** with the *c-myc* G-quadruplex to be $ca. (2 \pm 1) \times 10^7 \text{ dm}^3 \text{ mol}^{-1}$ based on two independent UV-visible titration experiments. The parent methylene blue compound displayed comparatively weaker binding affinities of $ca. 5 \times 10^6 \text{ dm}^3 \text{ mol}^{-1}$ for the *c-myc* G-quadruplex (Fig. S6, MB). We stress that due to the complicated DNA-binding behaviour of these compounds, the estimated binding constants are relative and not absolute values. To investigate the selectivity of **6b** for G-quadruplex DNA over duplex DNA, a parallel UV-visible absorption titration experiment with ct DNA was performed (Fig. S7). The K value of **6b** for ct DNA was estimated to be $9 \times 10^4 \text{ dm}^3 \text{ mol}^{-1}$ using two independent UV-visible titration experiments, which are at least one order of magnitude lower than the binding constants of **6b** for the *c-myc* G-quadruplex. By comparison, the binding affinity of MB for ct DNA was determined to be $ca. 5 \times 10^6 \text{ dm}^3 \text{ mol}^{-1}$ (Fig. S8), which is similar to the K value for the *c-myc* quadruplex and is consistent with previously reported binding constant of MB to ct DNA under a similar ionic strength [30]. Taken together, these data reveal that **6b** exhibits a ten-fold higher selectivity for G-quadruplex DNA over duplex DNA, whereas MB displays no significant selectivity for either structural form. This suggests that the introduction of side chains to the MB scaffold promotes *c-myc* G-quadruplex binding at the expense of duplex DNA binding, which is consistent with the

Binding Energies (kcal/mol)			
End-stacking at 3' (1) ^[a]	Intercalation near 3' (2) ^[a]	End-stacking at 5' (1) ^[a]	Intercalation near 5' (2) ^[a]
-49.87	32.79	-34.11	32.94

^[a] number of binding sites

molecular docking results (see above). Compounds **6b** exhibited constant molar extinction coefficients over the concentration ranges used in the absorption titration experiments.

3.7. Mass spectrometry

To examine the binding affinities of the MB derivative **6b** against other G-quadruplex structures, high resolution mass spectrometry was used. Solutions of the appropriate oligonucleotide were incubated in the presence of the MB derivative **6b** at room temperature for approximately 1 h. The mass spectra of the solution containing the oligonucleotide in the presence or absence of **6b** were then measured using ESI–TOF–MS and a representative example shown below in Fig. 8. In the mass spectrum of the *c-myc* G-quadruplex in the absence of **6b** (Fig. 8a), three peaks were identified, where each peak corresponds to the different ionization state of the *c-myc* G-quadruplex in the gas phase. Upon incubating the oligonucleotide with the methylene blue derivative **6b**, the resulting mass spectrum shows the appearance of additional peaks at 1556.2023, 1867.4318 and 1991.8289 mass units, which corresponds to the [1:1]⁶⁻, [1:1]⁵⁻ and [1:2]⁵⁻ *c-myc*–**6b** complex, respectively. The appearance of the additional peaks in the mass spectra indicates that the MB derivative **6b** is bound to the *c-myc* G-quadruplex.

By comparing the area under the peak associated with the free *c-myc* G-quadruplex and the *c-myc* G-quadruplex–**6b** complex in the mass spectrum, the relative binding affinity [31] can be estimated. It is important to note that the binding affinities determined using mass spectrometry are valid only in the gas phase and only serves as an approximation for solution state binding affinities. Repeating the mass spectrometry experiment with other biologically relevant G-quadruplex structures such as *c-kit* 1 (Fig. S9), *c-kit* 2 (Fig. S10) and *bcl-2* (Fig. S11), a series of relative binding affinities

Table 1

Relative affinity of MB **6b** with five intramolecular G-quadruplexes by ESI–TOF–MS analysis.

G-quadruplex sequence	Relative binding affinities
	Average (n = 2)
<i>c-myc</i> (27nt)	0.8604 ± 0.0125
<i>c-kit</i> 1 (27nt)	0.5681 ± 0.0038
<i>c-kit</i> 2 (27nt)	0.4249 ± 0.0078
<i>bcl-2</i> (27nt) ^a	0.4484 ± 0.0036

^a A truncated *bcl-2* sequence was used.

were determined and are summarized below in Table 1. Based on the relative binding affinities [31] estimated from the mass spectrometry experiments, it showed that the methylene blue derivative **6b** is selective towards the *c-myc* G-quadruplex with a measured binding affinity of 0.86, which is higher compared to the values determined for *c-kit* 1 (0.57), *c-kit* 2 (0.42) and *bcl-2* (0.45).

3.8. Inhibition of *c-myc* promoter activity in HepG2 cells

We next examined whether compound **6b** could inhibit *c-myc* gene promoter activity in cancer cells. Human hepatocarcinoma (HepG2) cells were transiently transfected with a Del 4 plasmid which harbours a 22-bp *c-myc* P1 promoter G-quadruplex forming sequence (5'-TG₄AG₃TG₄AG₃TG₄-3') upstream of the luciferase reporter gene [32]. Gratifyingly, addition of **6b** caused a dose-dependent decrease in luciferase activity with IC₅₀ = ca. 1 μM (Fig. 9). The induction or stabilization of the *c-myc* NHE III₁ G-quadruplex by the compound is expected to decrease the expression of luciferase as no inhibition (at concentrations up to

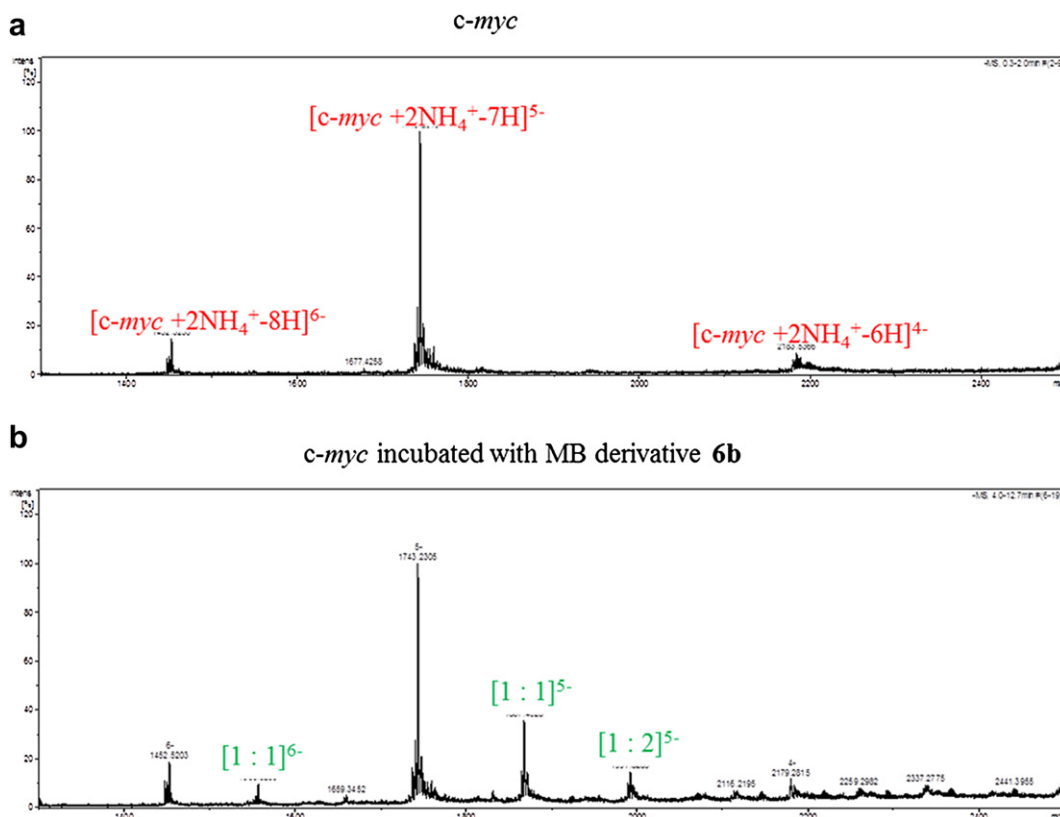


Fig. 8. ESI–TOF Mass spectra of: (a) the *c-myc* G-quadruplex; and (b) the *c-myc* G-quadruplex incubated in the presence of **6b** in ammonium acetate buffer (500 mM, pH 7.6).

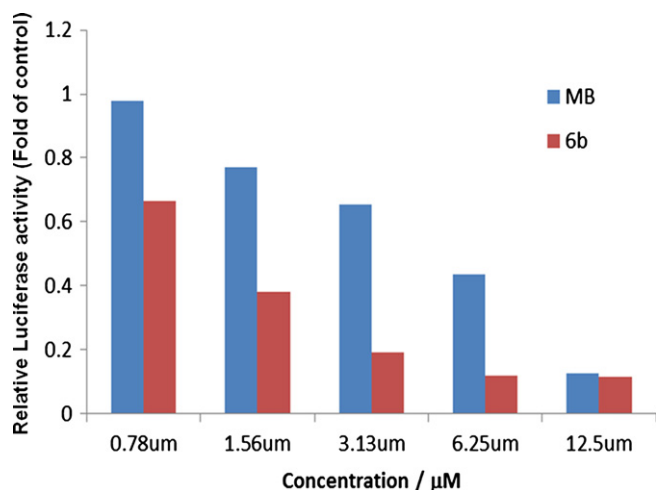


Fig. 9. Relative luciferase activity after the incubation of HepG2 cells transfected with the *c-myc* P1 promoter upstream of the luciferase reporter gene in the presence of different concentrations of **6b** and MB.

12.5 μM) was observed using the G4-mutant plasmid GM2 [33], which contained specific base substitutions (TGGGGAGGGTGAAGAGACTGGGGAAGG) that prevented the G-quadruplex formation (Fig. S12). By comparison, the initial lead compound MB appeared to be significantly less potent in this assay ($\text{IC}_{50} = ca. 6 \mu\text{M}$).

3.9. Cytotoxicity test (MTT assay)

We examined the cytotoxicity of compound **6b** using an MTT assay. Our results revealed that compound **6b** was toxic against the human cervical cancer (HeLa) cell line with an estimated IC_{50} value of 5 μM . By contrast, the cytotoxicity of the parent compound MB against HeLa cells was significantly lower ($\text{IC}_{50} = 15 \mu\text{M}$) in this assay. We hypothesize that the increased cytotoxicity of **6b** compared to MB against HeLa cells could be attributed, at least in part, to the inhibition of *c-myc* gene promoter activity through stabilization of the NHE III₁ G-quadruplex.

4. Conclusion

In conclusion, we have employed the unique intramolecular G-quadruplex *c-myc* NHE III₁ loop isomer model developed by our group to perform high-throughput virtual screening on an FDA-approved drug database of over 3000 compounds. Methylene blue emerged as an attractive scaffold for further structural modifications. As a proof-of-concept, we used a structure-based lead optimization approach to generate MB derivatives that displayed superior binding affinity and selectivity for the *c-myc* G-quadruplex over double-stranded DNA or other G-quadruplex structures. The binding of the compounds **6a–c** were initially investigated using fluorescence intercalator displacement and PCR-stop assay. Based on the results of the FID and the PCR-stop assay, the methylene blue derivative **6b** was found to be the most potent of the series consistent with the results of the molecular modeling. Mass spectrometry was also used to show that the MB derivative **6b** was selective towards the *c-myc* G-quadruplex over other biologically relevant G-quadruplexes such as *c-kit* 1, *c-kit* 2 and *bcl-2*. UV–visible spectroscopy was used to show that the MB derivative **6b** was selective towards G-quadruplex over ct DNA. We have demonstrated that **6b** could induce or stabilize *c-myc* G-quadruplex formation in both cell-free and cellular models. To our knowledge, this is the first large-scale application of high-throughput virtual

screening of an approved drug database for *c-myc* G-quadruplex stabilizing ligands. Given the selectivity of the methylene derivative of the *c-myc* G-quadruplex, there is considerable scope for further optimization of the MB core to improve the activity of the MB derivatives as G-quadruplex stabilizing compounds.

Acknowledgment

This work is supported by the Hong Kong Baptist University (FRG2/09-10/070 and FRG2/10-11/008), Centre for Cancer and Inflammation Research, School of Chinese Medicine (CCIR-SCM, HKBU) and City University of Hong Kong (Project No. 9667032).

Appendix. Supporting information

Supplementary data related to this article can be found online at doi:10.1016/j.biochi.2011.02.013.

References

- [1] T. Simonsson, G-quadruplex DNA structures - variations on a theme, *Biol. Chem.* 382 (2001) 621–628.
- [2] (a) J.-L. Mergny, C. Helene, G-quadruplex DNA: a target for drug design, *Nat. Med.* 4 (1998) 1366–1367; (b) J.L. Huppert, S. Balasubramanian, G-quadruplexes in promoters throughout the human genome, *Nucleic Acids Res.* 35 (2007) 406–413.
- [3] (a) L.H. Hurley, R.T. Wheelhouse, D. Sun, S.M. Kerwin, M. Salazar, O.Y. Fedoroff, F.X. Han, H. Han, E. Izbicka, H.D.D. Von, G-quadruplexes as targets for drug design, *Pharmacol. Ther.* 85 (2000) 141–158; (b) S.M. Kerwin, G-quadruplex DNA as a target for drug design, *Curr. Pharm. Des.* 6 (2000) 441–471; (c) T.-M. Ou, Y.-J. Lu, J.-H. Tan, Z.-S. Huang, K.-Y. Wong, L.-Q. Gu, G-quadruplexes: targets in anticancer drug design, *Chem. Med. Chem.* 3 (2008) 690–713; (d) D. Monchaud, M.-P. Teulade-Fichou, A hitchhiker's guide to G-quadruplex ligands, *Org. Biomol. Chem.* 6 (2008) 627–636; (e) S. Balasubramanian, S. Neidle, G-quadruplex nucleic acids as therapeutic targets, *Curr. Opin. Chem. Biol.* 13 (2009) 345–353; (f) C.A. De, L. Lacroix, C. Douarre, N. Temime-Smaali, C. Trentesaux, J.-F. Riou, J.-L. Mergny, Targeting telomeres and telomerase, *Biochimie* 90 (2008) 131–155; (g) S. Neidle, Human telomeric G-quadruplex: the current status of telomeric G-quadruplexes as therapeutic targets in human cancer, *FEBS J.* 277 (2010) 1118–1125.
- [4] D. Drygin, A. Siddiqui-Jain, S. O'Brien, M. Schwaebe, A. Lin, J. Bliesath, C.B. Ho, C. Proffitt, K. Trent, J.P. Whitten, J.K.C. Lim, H.D. Von, K. Anderes, W.G. Rice, Anticancer activity of CX-3543: a direct inhibitor of rRNA biogenesis, *Cancer Res.* 69 (2009) 7653–7661.
- [5] (a) C.V. Dang, K.A. O'Donnell, K.I. Zeller, T. Nguyen, R.C. Osthus, F. Li, The *c-Myc* target gene network, *Semin. Cancer Biol.* 16 (2006) 253–264; (b) K.I. Zeller, X. Zhao, C.W.H. Lee, K.P. Chiu, F. Yao, J.T. Yustein, H.S. Ooi, Y.L. Orlov, A. Shahab, H. Choong, Y. Fu, Z. Weng, V.A. Kuznetsov, W.-K. Sung, Y. Ruan, C.V. Dang, C.-L. Wei, Global mapping of *c-Myc* binding sites and target gene networks in human B cells, *Proc. Natl. Acad. Sci. U S A* 103 (2006) 17834–17839.
- [6] (a) E.H. Postel, S.E. Mango, S.J. Flint, A nuclease-hypersensitive element of the human *c-myc* promoter interacts with a transcription initiation factor, *Mol. Cell. Biol.* 9 (1989) 5123–5133; (b) T.L. Davis, A.B. Firulli, A.J. Kinniburgh, Ribonucleoprotein and protein factors bind to an H-DNA-forming *c-myc* DNA element: possible regulators of the *c-myc* gene, *Proc. Natl. Acad. Sci. U S A* 86 (1989) 9682–9686.
- [7] (a) A. Siddiqui-Jain, C.L. Grand, D.J. Bearss, L.H. Hurley, Direct evidence for a G-quadruplex in a promoter region and its targeting with a small molecule to repress *c-MYC* transcription, *Proc. Natl. Acad. Sci. U S A* 99 (2002) 11593–11598; (b) C.L. Grand, H. Han, R.M. Munoz, S. Weitman, H.D.D. Von, L.H. Hurley, D.J. Bearss, The cationic porphyrin TMPyP4 down-regulates *c-MYC* and human telomerase reverse transcriptase expression and inhibits tumor growth *in vivo*, *Mol. Cancer Ther.* 1 (2002) 565–573; (c) J. Seenisamy, S. Bashyam, V. Gokhale, H. Vankayalapati, D. Sun, A. Siddiqui-Jain, N. Streiner, K. Shinya, E. White, W.D. Wilson, L.H. Hurley, Design and synthesis of an expanded porphyrin that has selectivity for the *c-MYC* G-quadruplex structure, *J. Am. Chem. Soc.* 127 (2005) 2944–2959.
- [8] T.-M. Ou, Y.-J. Lu, C. Zhang, Z.-S. Huang, X.-D. Wang, J.-H. Tan, Y. Chen, D.-L. Ma, K.-Y. Wong, J.C.-O. Tang, A.S.-C. Chan, L.-Q. Gu, Stabilization of G-quadruplex DNA and down-regulation of oncogene *c-myc* by quindoline derivatives, *J. Med. Chem.* 50 (2007) 1465–1474.

- [9] P. Wu, D.-L. Ma, C.-H. Leung, S.-C. Yan, N. Zhu, R. Abagyan, C.-M. Che, Stabilization of G-Quadruplex DNA with platinum(ii) schiff base complexes: luminescent probe and down-regulation of c-myc oncogene expression, *Chemistry* 15 (2009) 13008–13021.
- [10] H.-M. Lee, D.S.-H. Chan, F. Yang, H.-Y. Lam, S.-C. Yan, C.-M. Che, D.-L. Ma, C.-H. Leung, Identification of natural product fonsicin B as a stabilizing ligand of c-myc G-quadruplex DNA by high-throughput virtual screening, *Chem. Commun.* 46 (2010) 4680–4682.
- [11] (a) D.W. Carley, Drug repurposing: identify, develop and commercialize new uses for existing or abandoned drugs. Part II, *Idrugs* 8 (2005) 310–313;
(b) C.R. Chong, D.J. Sullivan Jr., New uses for old drugs, *Nature* 448 (2007) 645–646;
(c) P. Schneider, Y. Tanrikulu, G. Schneider, Self-organizing maps in drug discovery: compound library design, scaffold-hopping, repurposing, *Curr. Med. Chem.* 16 (2009) 258–266.
- [12] J.A. DiMasi, R.W. Hansen, H.G. Grabowski, The price of innovation: new estimates of drug development costs, *J. Health Econ.* 22 (2003) 151–185.
- [13] (a) I.D. Kuntz, Structure-based strategies for drug design and discovery, *Science* 257 (1992) 1078–1082;
(b) J. Bajorath, Integration of virtual and high-throughput screening, *Nat. Rev. Drug Discov.* 1 (2002) 882–894;
(c) B.K. Shoichet, Virtual screening of chemical libraries, *Nature* 432 (2004) 862–865;
(d) D.S.-H. Chan, H.-M. Lee, F. Yang, C.-M. Che, C.C.L. Wong, R. Abagyan, C.-H. Leung, D.-L. Ma, Structure-based discovery of natural product-Like TNF- γ inhibitors, *Angewandte Chemie* 49 (2010) 2860–2864;
(e) C.-H. Leung, D.S.-H. Chan, H. Yang, R. Abagyan, D.-L. Ma, A natural product-like inhibitor of NEDD8-activating enzyme, *Chem. Commun* 47 (2011) 2511–2513;
(f) C.-H. Leung, D.S.-H. Chan, M.H.-T. Kwan, Z. Cheng, D.-L. Ma, Structure-based repurposing of FDA-approved drugs as TNF- inhibitors, *ChemMedChem.*(2011) DOI:10.1002/cmdc.201100016.
- [14] W.H. Bisson, A.V. Cheltsov, N. Bruey-Sedano, B. Lin, J. Chen, N. Goldberger, L.T. May, A. Christopoulos, J.T. Dalton, P.M. Sexton, X.K. Zhang, R. Abagyan, Discovery of antiandrogen activity of nonsteroidal scaffolds of marketed drugs, *Proc. Natl. Acad. Sci. U S A* 104 (2007) 11927–11932.
- [15] (a) J. Sambrook, E.F. Fritsch, T.E. Maniatis, *Molecular Cloning, a Laboratory Manual*, second ed. (1989) E.3 and E.10;
(b) G. Felsenfeld, S.Z. Hirschman, A neighbor-interaction analysis of the hypochromism and spectra of DNA, *J. Mol. Biol.* 13 (1965) 407–427.
- [16] K. Suntharalingam, A.J.P. White, R. Vilar, Two metals are better than one: investigations on the interactions between dinuclear metal complexes and quadruplex DNA, *Inorg. Chem.* 49 (2010) 8371–8380.
- [17] C.V. Kumar, E.H. Asuncion, DNA binding studies and site selective fluorescence sensitization of an anthryl probe, *J. Am. Chem. Soc.* 115 (1993) 8547–8553.
- [18] O.M. New, D. Dolphin, Design and synthesis of novel phenothiazinium photosensitizer derivatives, *Eur. J. Org. Chem.* (2009) 2675–2686.
- [19] (a) T.B. Lanni, K.L. Greene, C.N. Kolz, K.S. Para, M. Visnick, J.L. Mobley, D.T. Dudley, T.J. Baginski, M.B. Liimatta, Design and synthesis of phenethyl benzo[1,4]oxazine-3-ones as potent inhibitors of PI3Kinase γ , *Bioorg. Med. Chem. Lett.* 17 (2007) 756–760;
(b) A.R. Thornton, V.I. Martin, S.B. Blakey, π -Nucleophile traps for metal-lonitrene/alkyne cascade reactions: a versatile process for the synthesis of α -aminocyclopropanes and β -aminostyrenes, *J. Am. Chem. Soc.* 131 (2009) 2434–2435.
- [20] A.H. Lewin, H.A. Navarro, S.W. Mascarella, Structure-activity correlations for β -phenethylamines at human trace amine receptor 1, *Bioorg. Med. Chem.* 16 (2008) 7415–7423.
- [21] L. Strekowski, D.F. Hou, R.L. Wydra, R.F. Schinazi, A synthetic route to 3-(dialkylamino)phenothiazin-5-ium salts and 3,7-disubstituted derivatives containing two different amino groups, *J. Heterocycl. Chem.* 30 (1993) 1693–1695.
- [22] (a) M. Totrov, R. Abagyan, Flexible protein-ligand docking by global energy optimization in internal coordinates, *Proteins* (1997) 215–220 Suppl. 1;
(b) D.-L. Ma, T.-S. Lai, F.-Y. Chan, W.-H. Chung, R. Abagyan, Y.-C. Leung, K.-Y. Wong, Discovery of a drug-like G-quadruplex binding ligand by high-throughput docking, *ChemMedChem.* 3 (2008) 881–884.
- [23] G.N. Parkinson, M.P.H. Lee, S. Neidle, Crystal structure of parallel quadruplexes from human telomeric DNA, *Nature* 417 (2002) 876–880.
- [24] A. Ambrus, D. Chen, J. Dai, R.A. Jones, D. Yang, Solution structure of the biologically relevant G-quadruplex element in the human c-myc promoter. Implications for G-quadruplex stabilization, *Biochemistry* 44 (2005) 2048–2058.
- [25] (a) S.L. Narsapur, G.J. Naylor, Methylene blue. A possible treatment for manic depressive psychosis, *J. Affect. Disord.* 5 (1983) 155–161;
(b) J. Clutton-Brock, Two cases of poisoning by contamination of nitrous oxide with higher oxides of nitrogen during anaesthesia, *Br. J. Anaesth.* 39 (1967) 388–392;
(c) J. Clifton 2nd, J.B. Leikin, Methylene blue, *Am. J. Ther.* 10 (2003) 289–291;
(d) M. Wainwright, L. Amaral, The phenothiazinium chromophore and the evolution of antimalarial drugs, *Trop. Med. Int. Health* 10 (2005) 501–511;
(e) J.P. Tardivo, G.A. Del, d.O.C. Santos, D.S. Gabrielli, H.C. Junqueira, D.B. Tada, D. Severino, R.d.F. Turchiello, M.S. Baptista, Methylene blue in photodynamic therapy: from basic mechanisms to clinical applications, *Photodiagnosis Photodyn. Ther.* 2 (2005) 175–191.
- [26] H. Sun, J. Xiang, Y. Zhang, G. Xu, L. Xu, Y. Tang, Spectroscopic studies of the interaction between methylene blue and G-quadruplex, *Chin. Sci. Bull.* 51 (2006) 1687–1692.
- [27] P. Ragazzon, J.B. Chaires, Use of competition dialysis in the discovery of G-quadruplex selective ligands, *Methods* 43 (2007) 313–323.
- [28] J. Seenisamy, E.M. Rezler, T.J. Powell, D. Tye, V. Gokhale, C.S. Joshi, A. Siddiqui-Jain, L.H. Hurley, The dynamic character of the G-quadruplex element in the c-MYC promoter and modification by TMPyP4, *J. Am. Chem. Soc.* 126 (2004) 8702–8709.
- [29] Y. Wang, A. Zhou, Spectroscopic studies on the binding of methylene blue with DNA by means of cyclodextrin supramolecular systems, *J. Photochem. Photobiol. A Chem.* 190 (2007) 121–127.
- [30] M. Hossain, P. Giri, G.S. Kumar, DNA intercalation by quinacrine and methylene blue: a comparative binding and thermodynamic characterization study, *DNA Cell Biol.* 27 (2008) 81–90.
- [31] L.-P. Bai, M. Hagihara, Z.-H. Jiang, K. Nakatani, Ligand binding to tandem G quadruplexes from human telomeric DNA, *ChemBioChem* 9 (2008) 2583–2587.
- [32] T.-C. He, A.B. Sparks, C. Rago, H. Hermeking, L. Zavel, C.L.T. Da, P.J. Morin, B. Vogelstein, K.W. Kinzler, Identification of c-MYC as a target of the APC pathway, *Science* (Washington, D. C.) 281 (1998) 1509–1512.
- [33] R.K. Thakur, P. Kumar, K. Halder, A. Verma, A. Kar, J.L. Parent, R. Basundra, A. Kumar, S. Chowdhury, Metastases suppressor NM23-H2 interaction with G-quadruplex DNA within c-MYC promoter nuclelease hypersensitive element induces c-MYC expression, *Nucleic Acids Res.* 37 (2009) 172–183.